Peer-reviewed version available at Materials 2018, 11, 2477; doi:10.3390/ma11122477

Article

Damage Determination in Ceramic Composites Subject to Tensile Fatigue Using Acoustic Emission

Gregory N. Morscher [1]* and Zipeng Han [2]

[1] Department of Mechanical Engineering; University of Akron, Akron, Oh; gm33@uakron.edu
[2] Department of Mechanical Engineering; University of Akron, Akron, Oh; zh10@zips.uakron.edu
* Correspondence: gm33@uakron.edu; Tel.: +01-330-972-7741

Abstract: Acoustic emission (AE) has proven to be a very useful technique for determining damage in ceramic matrix composites (CMCs). CMCs rely on various cracking mechanisms which enable non-linear stress-strain behavior with ultimate failure of the composite due to fiber failure. Since these damage mechanisms are all micro-fracture mechanisms, they emit stress waves ideal for AE monitoring. These are typically plate waves since for most specimens or applications one dimension is significantly smaller than the wavelength of the sound waves emitted. By utilizing the information of the sound waveforms captured on multiple channels from individual events, the location and identity of the sources can often be elucidated. The keys to the technique are the use of wide-band frequency sensors, digitization of the waveforms (modal AE), strategic placement of sensors to sort the data and acquire important contents of the waveforms pertinent for identification, and familiarity with the material as to the damage mechanisms occurring at prescribed points of the stress history. The AE information informs the damage progression in a unique way which adds to the understanding of the process of failure for these composites. The AE methodology was applied to composites tested in fatigue at different frequencies where identification of when and where AE occurred coupled with waveform analysis leads to source identification and failure progression.

Keywords: Acoustic emission, ceramic matrix composites, matrix cracking, fiber breakage

1. Introduction

Ceramic matrix composites (CMCs) comprised of continuous ceramic fibers and ceramic matrices possess high temperature capability and offer higher toughness as compared to monolithic ceramic materials [1]. This is highly desired in such applications such as hot-section jet engine components where the additional toughness enables some ease in design [2]. The mechanism for enhanced toughness in properly designed CMCs is the enabling of matrix micro-fractures due to a weak interface or layer that exists between the fiber and the matrix [3]. For example, when a crack initiates under a tensile load at a local flaw source, it debonds along the fiber in this weak interface region and propagates past fibers leaving fibers to bridge the crack wake. The strong fibers in the fiber-bridged transverse matrix crack will carry the load shed from the matrix until the applied load is sufficient to fail the fibers in a local region. The result is local strain and non-linear stress-strain behavior. Ultimate failure then is controlled by the failure of the fibers which are bridging the matrix cracks at a higher stress.

Acoustic emission (AE) is an excellent technique to monitor the micro-fracture damage mechanisms in fiber-reinforced CMCs. Since these mechanisms are all micro-fracture events, part of the energy release that happens when they occur will be in the form of sound (stress) waves transmitted through the material. In reality there are thousands of micro-fracture events which occur during the tensile stress-strain response of a CMC. The uniqueness of AE is that it is a passive technique, there is no input, one just listens to what the material tells you. In this sense one is taking advantage of a "smart sensing" approach to material damage accumulation. Ideally one would like to be able to monitor when such events occur, what specific type of event occurred and where that

Peer-reviewed version available at Materials 2018, 11, 2477; doi:10.3390/ma11122477

event occurred in the volume of interest. AE can or at least has the potential to inform in all three of these areas.

The utility of AE to identify the onset of micro-fracture damage has been demonstrated in a number of studies. First and foremost, AE is probably the best technique to distinguish when initial micro-fracture damage occurs. This has been demonstrated for CMCs throughout the years [4-6]. Initial transverse cracking in CMCs is typically small and not detected from non-linearity in the stress/strain curve; therefore, graphical constructs such as offset stress methods to determine "first cracking stress" are insufficient [7]. Since initial microcracks in CMCs do not result in a change in the elastic modulus, ultrasonic NDE approaches are not capable of detecting initial damage and since the initial microcracks are typically very small (e.g., 90 two tunnel cracks [8]), x-ray and thermographic techniques are also incapable of detecting this initial damage. One significant application of this finding is that the stress to cause these initial microcracks correlates with the stress for long-time creep-rupture [9], i.e., the flaw that would initiate a slow-crack growth mechanism controlled failure crack at elevated temperatures under a constant stress load.

Second, AE has been used effectively in matrix-dominated CMCs [10] during tensile fast-fracture type tests. In these systems, the AE energy of the waveforms is directly related to matrix crack density for both melt-infiltrated [11] and chemically vapor infiltrated matrix SiC fiber-reinforced, SiC matrix composites [12].

Third, AE has been used effectively to locate sources of damage with a resolution of less than ~ 0.5 mm. This was beneficial in identifying which part of the architecture transverse cracking occurred in for a 3D orthogonal SiC/SiC composite [13], where cracks emanated from a notch tip with increasing load [14], and how far cracks propagated around a C-coupon during an interlaminar tension test [15]. More recently, the location analysis coupled with the frequency analysis has enabled the location of transverse crack propagation emanating from a single notch that occurred in the interior (tunnel) plies of a composite and the exterior (surface extending) plies of a composite in a laminate SiC/SiC composite [16].

Fourth, AE has been used to identify sources (mechanisms) based on their waveform characteristics. Already mentioned was high energy which has been shown to correlate with matrix cracks for tensile tests. In addition, energy content coupled with frequency content has been shown to correlate with interior cracks (high frequency – low energy) versus surface extending cracks (low frequency - high energy) [16-18]. This was based on an understanding of plate-wave theory [19-20] where surface cracks being off-center of the midline of a specimen would promote anti-symmetric low frequency flexural waves (which are usually higher in energy for thin plates especially when sensors are mounted on the surface of the specimen) and internal mode 1 cracks being on or near the center line of the composite would promote symmetric extensional waves which always have higher frequencies than flexural waves. This was first demonstrated for the same type of mechanism (transverse cracks at the surface and in the interior) in polymer laminate composites [17-18] and later in SiC/SiC laminate composites [16].

Based on the understanding and methodology described above for waveform-based AE, this study is aimed at utilizing these techniques to understand damage development for a conventional dogbone SiC/SiC composite when tested under tensile-tensile fatigue conditions of different frequencies.

2. Materials and Methodology

The materials and fatigue tests evaluated in this work were from another study [21-22]. However, this study uses the data generated from that study to analyze the AE data more in-depth. The SiC/SiC composites evaluated were of the woven fiber-reinforced slurry-derived melt infiltrated variety. The composites were fabricated by Goodrich Inc. (Santa Fe Springs, CA) prior to their acquisition by United Technologies. The composites were made up of eight plies of 0/90 woven five-harness satin cloth of Hi-Nicalon Type S (Nippon Carbon, Tokyo Japan) fibers. A boron nitride interphase of approximately 0.5 microns followed by a chemically vapor deposited SiC layer of approximately 2-3 microns was infiltrated to rigidize the structure. This was followed by SiC particle

infiltration via an aqueous slurry. After drying the slurry infiltrated preform, the preform was infiltrated with molten Si so that much of the open porosity was filled with Si. It should be noted that these panels had some excess porosity. Fatigue tests were performed at 0.01, 0.1 and 1 hz at an R value of 0.1 at room temperature using an MTS hydraulic universal testing machine outfitted with hydraulic grips, a 25.4 mm clip on extensometer (2% max strain). Table 1 lists some physical and mechanical properties and test data for all the specimens. Note that some of the specimens were subject to increasing peak-stress fatigue steps if they did not fail after some amount of time. The ratio R was 0.1 and was always maintained for increasing peak stresses. The specimens were also monitored for electrical resistance change which will not be discussed here, having been the major topic of the earlier work [18].

Table 1. Physical and Mechanical Properties of Specimens Tested.

Specimen	Fiber fraction	E, GPa	Frequency, hz	Peak Stress, MPa
111-8	0.238	206	0.1	140; 150
111-9	0.26	221	0.01	140; 170; 180; 190; 200
113-3	0.236	185	0.1	140
113-9	0.246	226	1	140; 150
147-3	0.258	248	1	180

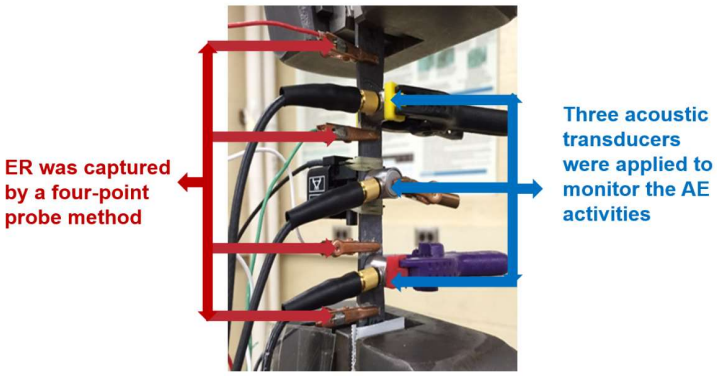

Figure 1: Test set-up for tensile fatigue tests showing three AE sensors and electrical resistance leads (not part of this study).

Acoustic emission was monitored using a Digital Wave Fracture Wave Detector (Centennial, CO. USA). The test set up is shown in Figure 1. Three wide-band (50 to 2,000 khz) B1025 Digital Wave AE sensors were applied to the face of the specimen using plastic spring clamps. The outer sensors were separated by 60 mm with the third sensor half way in between. For this AE system, the sensors are all "enslaved" meaning that when one sensor triggers all of the sensors capture and record the waveform on the given channel at exactly the same time. Therefore for a given event there are three waveforms. In this way, the data can be easily sorted so that only AE data that triggers the middle sensor (sources closest to the middle sensor, i.e., in the gage section of the specimen) is used in the analysis. This is critical since it is not unusual for significant AE activity to emanate from the grips for CMCs. The AE waveform set-up was 1024 or 2048 points, 10 Mhz sampling rate, and 25% pretrigger. A 20 dB preamplifier was also used.

Post-test analysis of the AE data was performed using the Digital Wave *WaveExplorer* software to determine the waveform energies. The waveform data was also imported into a MATLAB file in order to determine the frequency centroid for each waveform and to determine the time of arrival for location analysis using the AIC method [23, 24]. The location along the length utilized the time of arrival on the outermost sensors and the speed of sound as determined by events which occurred in

Peer-reviewed version available at Materials 2018, 11, 2477; doi:10.3390/ma11122477

the grip region and crossed the outer two sensors during the test [6]. However, when exact location was required for certain sets of data, manual inspection of waveforms to obtain peak values were employed.

3. Results

The stress-step fatigue and AE history are shown in Figure 2. Two of the tests had only one peak stress condition prior to failure whereas the other three specimens had at least two peak stress steps as indicated by the stress jumps in Figure 2a. The AE activity is plotted as cumulative AE energy, which has been found to correlate well with transverse matrix crack density [11-12]. Note also that for the AE activity, there is a jump in energy accumulated for each stress jump which corresponds to the initial loading of the specimen upon the first cycle of the higher peak stress condition.

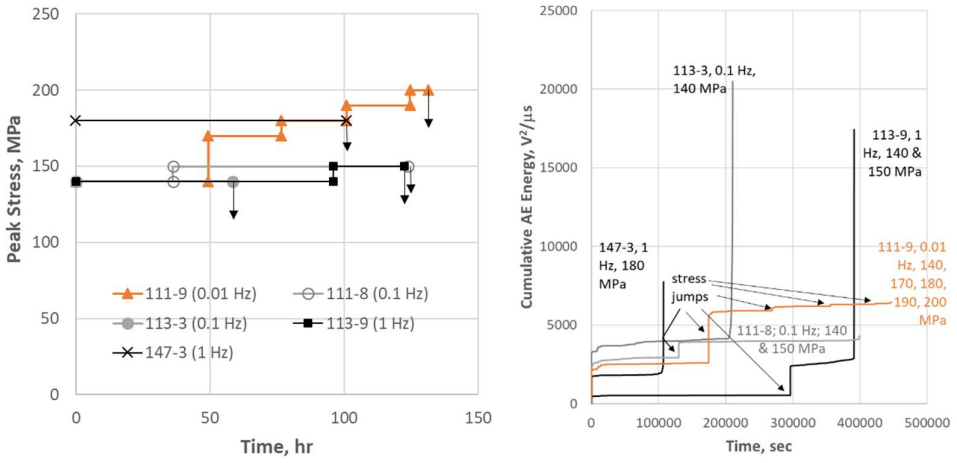

(a) (b)

Figure 2. The history of stress condition and AE activity for the CMC specimens: (**a**) peak stress plotted versus time for R = 0.1 fatigue cycles where the downward arrow indicates failure and (**b**) cumulative AE energy versus time for each specimen.

Typically for these types of composites, most of the AE energy occurs on loading and not near failure. The rationale for this is that large transverse matrix cracks which occur over the entire gage section create considerable energy since they are of large area and high modulus. When the crack forms and propagates, considerable surface energy is created from hundreds of cracks (several per mm in multiple plies) during the loading of the specimen. Failure in a typical tensile test for these types of composites would mostly involve fiber failure, which are of significantly smaller cross-sectional area and are only located within a narrow region of the gage section. A striking feature for some of the fatigue specimens in this study is that several of the specimens showed more AE energy cumulated at the end of the test than the entire stress history that precedes it. However, two of the tests did show only a minor increase in AE activity at failure as is typical of these types of composites when tested to failure in tension. It is apparent that the specimens which showed dramatic increase in AE at failure were tested at higher frequencies tests (two 1 Hz and one 0.1 Hz) whereas the two specimens that did not show this behavior were at lower frequencies (one 0.1 and one 0.01 Hz). In order to understand what was causing the difference in AE behavior, the methodology for AE analysis described above was employed with some microstructural analysis to correlate AE activity with the damage mechanisms that developed during the tests.

3.1. AE Fatigue Cycle Analysis

The set-up for AE acquisition was such that the parametrics (load and strain) were acquired every second in addition to the AE waveforms. Thus, the variation in stress for a given fatigue cycle was not possible for the 1 Hz data. But for the 0.1 Hz and 0.01 Hz tests, enough load data was available

Peer-reviewed version available at Materials 2018, 11, 2477; doi:10.3390/ma11122477

to discern at which point of the cycle the events were occurring. The AE analysis for the 0.1 Hz test (113-3) will be presented here in detail which showed the enhanced AE activity near failure (Figure 2b). The features found for the 0.1 Hz test were also observed for the 1 Hz tests (147-3 and 113-9[1]) for the most part. Where there were differences is discussed below.

The AE data was separated into events which occurred near the peak of the cycle and event which occurred near the valley of the cycle. Figure 3a shows the cumulative AE energy data for the overall test as well as the contributions of energy for the peak and valley. There were no valley events until the 201,990 second (56.1 hour) mark of the test, 2.4 hours prior to failure. After the occurrence of valley events, most of the AE energy was dominated by what occurred during the valley part of the stress-cycles with some appreciable AE occurring during the peak of the cycle as well. An example of when the valley and peak events occur in a stress cycle is shown in Figure 3b for the cycle centered at 210,001 seconds. Note that "valley" events occur during unloading as the valley is approached and "peak" events occur upon loading as the peak of the stress-cycle is approached.

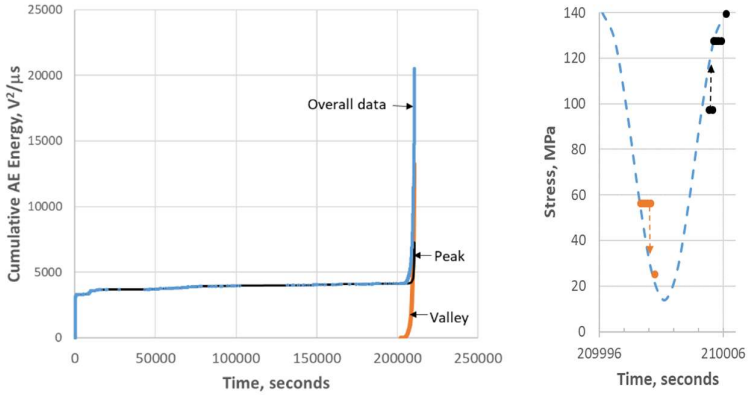

(a) (b)

Figure 3: (a) Cumulative AE energy for 113-3 (0.1 Hz fatigue). The "Overall data" is separated into the part of the data that occurred during the peak of the fatigue cycles and the data that occurred during the valley. (b) A stress cycle near the end of the test showing the occurrence of the "valley" (unload) events and the "peak" (reload) events. Note that the AE acquisition software only captured the load data every second so the events to the right of the stress curve should be displaced downwards for valley events and upward for peak events onto the stress line.

To understand the intensity and progression of peak and valley events an energy analysis was performed. For each event the average energy was determined by taking the average of the energies of the two outer sensors. Figure 4 shows the AE event energy versus time for the entire test that were added in sequence to produce Figure 3. Each data point represents a single AE event from a discrete source. Significant AE activity occurs at the beginning of the test, primarily in the first few cycles. For most of the test little AE occurs until the very end of the test. The energy ranges from 0.1 to 50 $V^2/\mu s$ until near the end of the test where energies less than 0.01 $V^2/\mu s$ were recorded. Since the valley events were only observed at the end of the test (201,990 seconds), the peak and valley events were plotted separately after 200,000 seconds in Figure 4b and 4c, respectively. There were 2,156 valley events compared to 1,367 events over this time period. Valley events were also much more prevalent prior to about 206,000 seconds. It is also obvious that the valley events tended to be of higher energy than the peak events though both peak and valley showed increasing energy events as

[1] Though both specimens were tested at 1 Hz, the peak and valley events described in the following could be discerned by the timing of the event. In other words, the peak and valley events occurred approximately 0.5 seconds from one another.

Peer-reviewed version available at Materials 2018, 11, 2477; doi:10.3390/ma11122477

time progressed. The peak events contained low and high energies (Figure 4b), including nearly all the very low energy events at the end of the test.

To understand the relationship of valley and peak AE events, the number of events per cycle were counted for valley and peak events for the time range greater than 200,000 seconds (Figure 5). It should be noted that prior to this time, most cycles did not even have one AE event except for the beginning of the test. Figure 5 shows that there were more valley events per cycle than peak events until very near failure (~ 12th last cycle). Therefore, it is apparent that whatever is happening upon unloading causes or at least contributes to what happened upon loading during the fatigue cycles. Since there is a preponderance of unloading (valley) events at the onset of this high AE activity region approaching the end of the test (Figure 4c), it appears to precipitate the subsequent intensity of sources causing AE during the loading (peak) part of the cycle. To better understand the nature of what is causing the AE events a location and frequency analysis was performed.

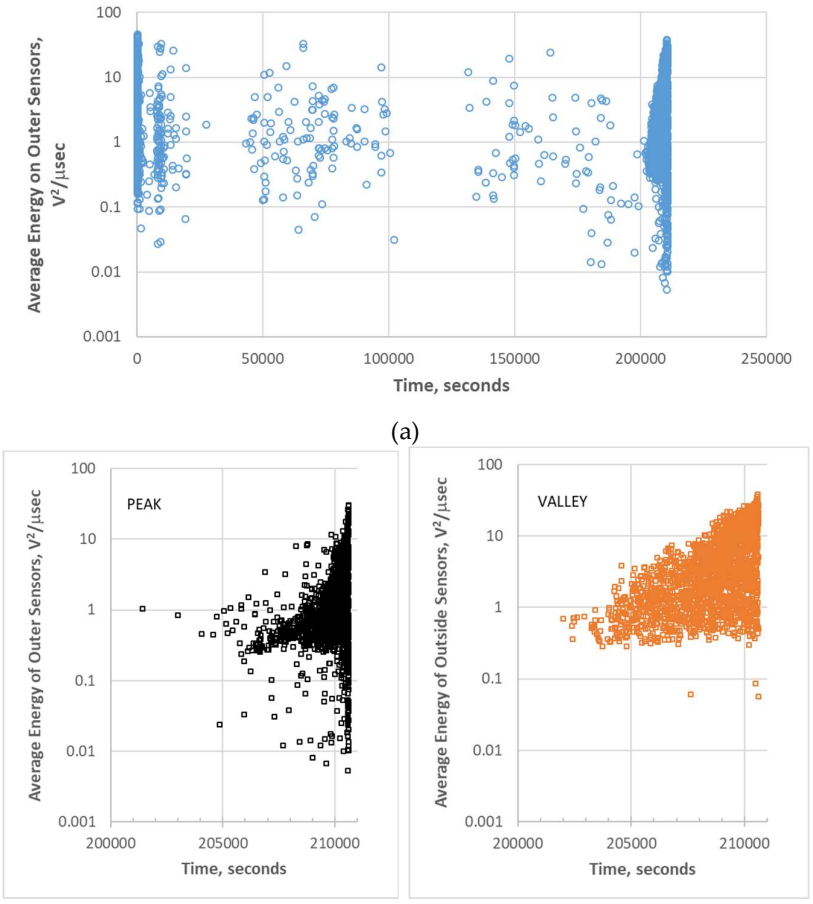

Figure 4: Average energy per event of 113-3 (a) for the entire test, (b) for peak events at the end of the test and (c) for valley events at the end of the test.

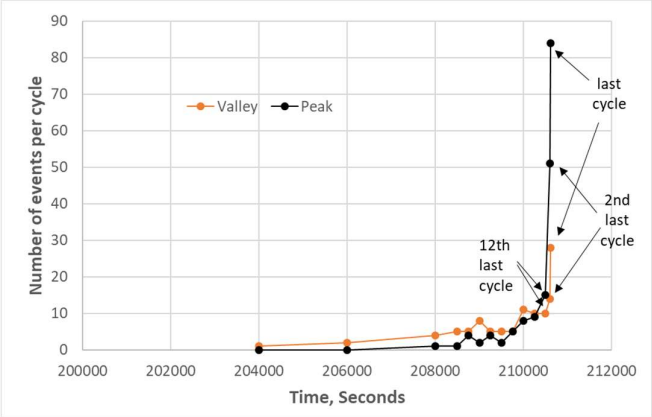

Figure 5: Number of events per cycle for peak and valley events for 113-3 at the end of the test.

3.2 AE Event Location Analysis

The original AE data was sorted selecting only the AE events that triggered the middle sensor. However, to get accurate location, the difference in times of arrival of the two outer sensors, Δt, is required and one needs to account for the changing speed of sound during the test [6,24]. The speed of sound can be accounted for as the test progressed by determining the time it took sound to travel between the two outer sensors, Δt_x, from events which occurred in the grips. Since there was a period of no AE activity prior to the 130,000 second mark (Figure 4a), only the data after 130,000 was analyzed for location leading up to failure. The time of arrival for a given event was determined manually to achieve the most accurate location analysis possible [13]. Examples of valley and peak waveforms are shown in Figure 6 with arrows indicating first peaks. Note that the first peak for the valley event on the top and bottom sensor is negative and the first peak for the peak event is positive – this is significant and will be explained below.

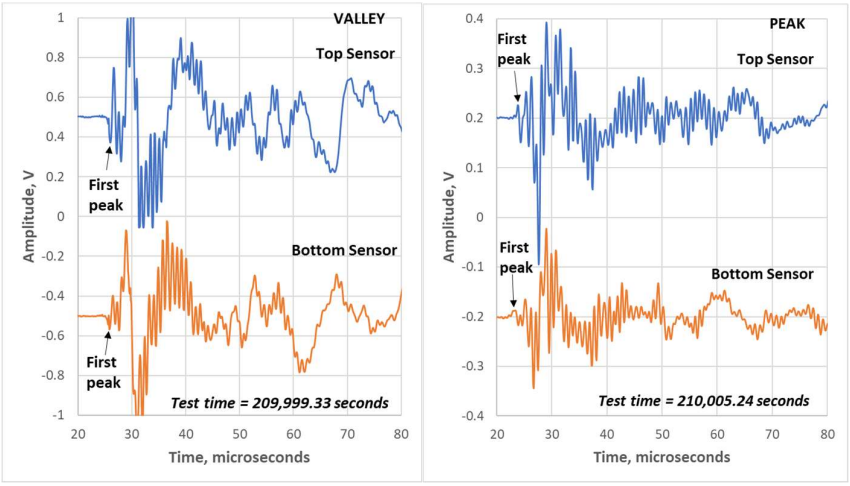

(a) (b)

Figure 6: Waveforms from top and bottom sensors for a (a) valley event and a (b) peak event showing the first peaks of each waveform from 113-3.

From the determination of first peak times of arrival, the location can be determined from:

$$\text{Location} = (x/2)(\Delta t/\Delta t_x) \quad (1)$$

Where x is the length between the outer sensors (25 mm). The location of each event after 130,000 seconds is plotted in Figure 7a versus the time of the test where the value 0 is the center of the gage

Peer-reviewed version available at Materials 2018, 11, 2477; doi:10.3390/ma11122477

section. Each datapoint represents a single event and the width of the datapoint is proportioned to the average AE energy of the given event. There are scattered and infrequent peak events for the over 70,000 seconds (~ 20 hours) leading up to the heightened period of AE activity just prior to failure. The events at the end of the test are so dense that the period after 200,000 seconds (box in Figure 7a) were plotted in Figure 7b and 7c for the valley and peak events, respectively. Most of the peak and all of the valley events are concentrated in the 0 to +1.5 mm location from the center of the gage, which is where failure took place. Whatever occurred just prior to failure would not correspond to distributed matrix cracking along the gage length. Therefore, one would expect to observe localized damage near the fracture surface within an approximate 2 mm length or less of the composite as will be shown below.

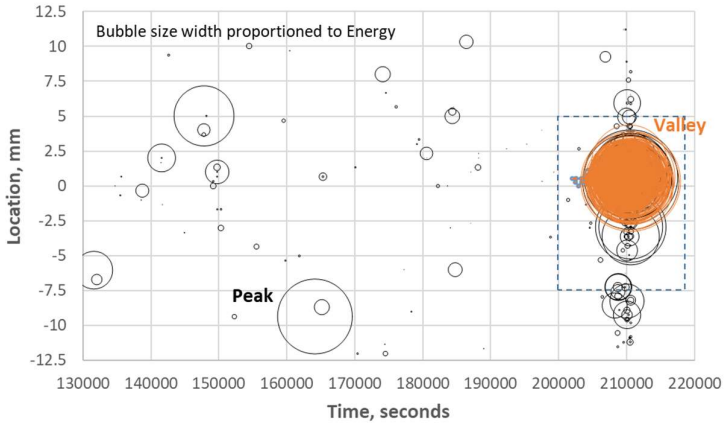

(a)

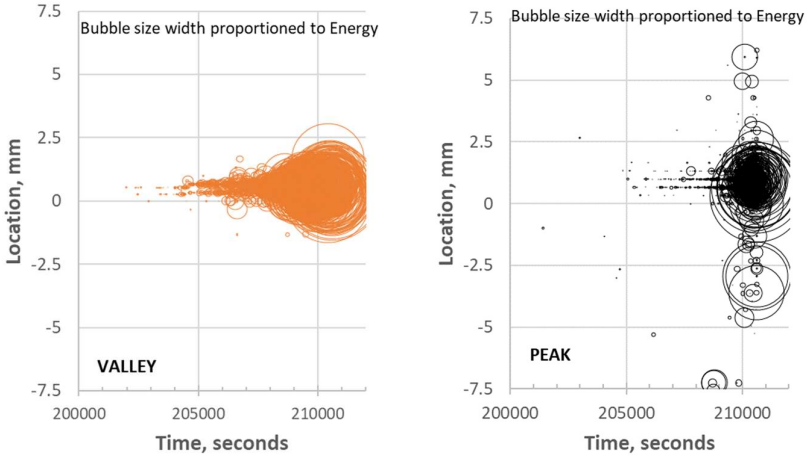

(b) (c)

Figure 7: AE location analysis distinguishing between "peak" and "valley" events for (a) the last half of the test and for the (b) valley and (c) peak events for the last ~ 3 hours of the test for 113-3.

3.3 AE Waveform Analysis

In earlier studies [16-18,25] it was found that frequency content was often helpful in identifying some micro fracture mechanisms such as matrix cracks and fiber fractures as well as the location of matrix cracks, e.g., surface versus internal. The frequency centroid has been a useful parameter to assess the frequency content of waveforms for this purpose [18,20]. Figure 8 shows the waveform and Fast Fourier Transform (FFT) for the same events as Figure 6 except for the middle sensor 3. It has been shown that higher frequencies do not transmit over longer distances effectively in these types of composites [18], so the sensor closest to the source (middle) is used for frequency analysis. Also

Peer-reviewed version available at Materials 2018, 11, 2477; doi:10.3390/ma11122477

shown in Figure 9 for the waveform/FFT of the two events in is the frequency centroid (FC). Note that the valley event (Figure 8a) has a frequency centroid about 200 kHz lower than that of the selected peak event (Figure 8b). The frequency centroids of all the valley and peak events are plotted in Figure 9 for the last few hours of the test.

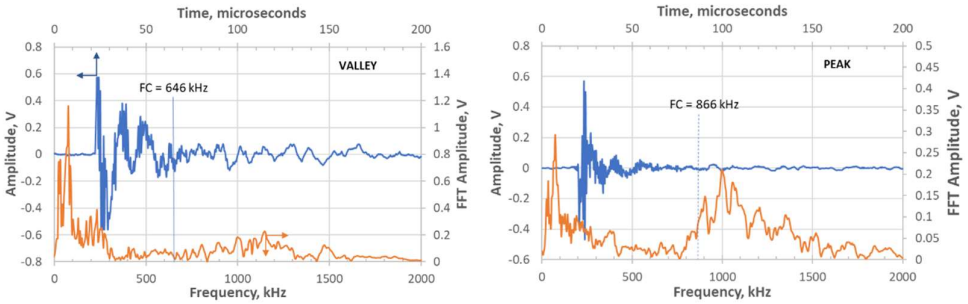

(a) (b)

Figure 8: Waveform and Fast Fourier Transform (FFT) of sensor 3 waveform for the same waveforms in Figure 7: (a) valley event at 209,999.33 seconds and (b) peak event at 210,005.24 seconds during the test.

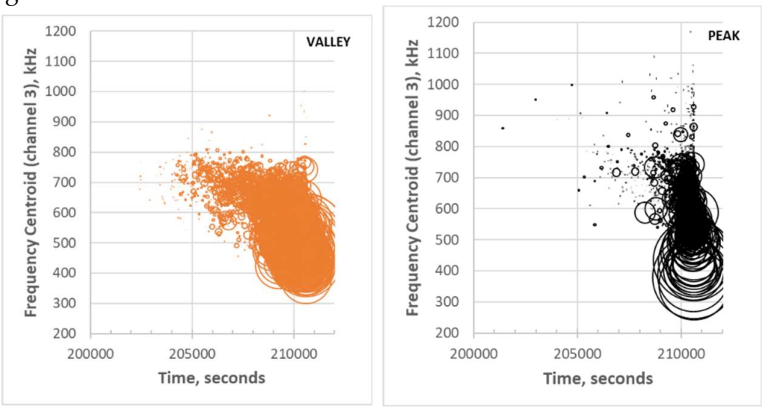

(a) (b)

Figure 9: Frequency centroids for (a) valley and (b) peak events at the end of the test. Note that the bubble width is normalized to AE energy of the waveform.

Valley events dominate at first near the end of the test (~ 202,000 seconds) and increase in number, frequency range (especially lower frequency content) and energy range (especially higher energy events) with time. Valley events are also characterized by the first peak being negative (Figure 6a) when measured in the far field (sensors 1 and 2). This points to whatever is happening in the valley as being compressive. When a compressive force causes a microfracture event such as a longitudinal crack, something being crushed, or a shear crack, the front of the waveform, an extensional wave, will be in tension (negative direction for surface transducer)[2]. All of the valley events showed this negative first peak on the far sensors. Note that the near sensor in Figure 8a

[2] In large semi-infinite structures such as bridges or the earth, AE events emanating from shear can give positive or negative first peaks depending on the location of the sensor with respect to the shear direction (if ahead of the source and in the shear direction, positive, and if behind the source and opposite the shear direction, negative) [26]. However, for a plate, the extensional wave is not like a P-wave in the semi-infinite case and the direction of the first peak would be dictated by the direction of strain response. For example if a transverse crack forms in tension or a fiber breaks in tension, the direction of material response (spring back) would be outward, away from the original location, and "push" the material in compression outward resulting in the front end of the stress wave being positive. The opposite would be true for a compressive mechanism regardless of the mechanism itself (e.g., longitudinal split, shear or crushing).

Peer-reviewed version available at Materials 2018, 11, 2477; doi:10.3390/ma11122477

shows a positive first peak for the valley event. Some valley events showed positive and other events showed negative first peak. Since the sensor is essentially on top of the source location, the first peak is dominated by the flexural wave since the waveform does not have enough distance to travel to separate itself from the flexural (the wavelengths of the extensional and flexural are approximately 1.5 to 2 cm). Therefore, the sign of the first peak on the middle sensor probably is indicative of the direction of flexure of the specimen caused by the stress wave and is perhaps related to the "side" of the specimen that the damage event occurred.

Peak events at the end of the test are characterized by a positive first peak (Figure 6b). This would be indicative of a tensile force causing the microfracture event resulting in the front of the extensional component of the stress wave being in compression. For this specimen, peak events occur later in time (> 205,000 seconds) than the onset of the valley events. This means that a significant number of valley events occurred for about an hour prior to the onset of significant peak event formation. The number, frequency range and energy range of the peak events also increase with time as failure is approached (Figure 9b). The peak event frequency range though is much broader and there are a number of very high frequency content events prior to failure.

3.4 Microstructural Analysis

A polished section of the fracture surface for 113-3 is shown in Figure 10. Near the fracture surface there is considerable cracking phenomena. Not only are there transverse cracks, there are a significant number of longitudinal and diagonal oriented cracks, especially in the 90 fiber tow regions. Some arrows are provided to highlight these types of cracks. This region of damage is on the order of 1 mm from the fracture surface itself. For the polished section far from the fracture surface, the average transverse crack spacing is ~ 1 crack per mm and there is no evidence for concentrated damage in 90 fiber tow regions. It is also interesting that there is significant transverse matrix cracking near the fracture surface with much smaller crack spacing than the far field. Therefore, it is reasonable to assume that the AE events which occur near the fracture surface location correspond to the increased damage observed in the polished section.

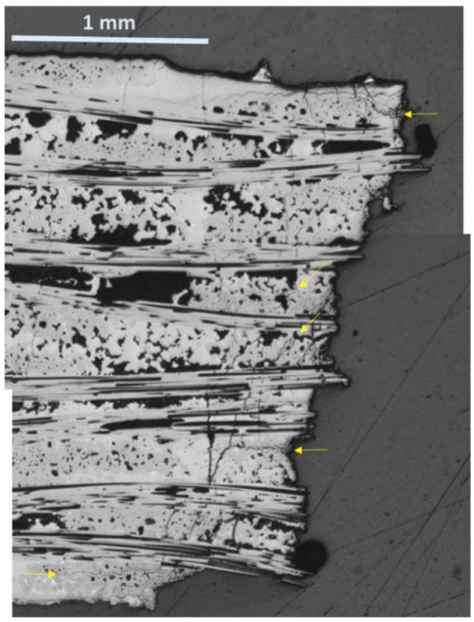

Figure 10: Polished longitudinal sections of CMC specimens near fracture surface for showing increased damage regions near fracture surface for (a) 113-3

Two inferences can be made from these observations:

- The unique damage to the fracture surface region appears to be associated with 90 tow longitudinal and diagonal shear type cracking. The 90 tow region is the weakest region within these types of composites since the BN fiber interphase that separates the fibers from the CVI portion of the matrix is a weak layer resulting in easy crack propagation parallel to the fiber direction. In addition, there is porosity within the tow which would offer stress-concentrator sites for crack initiation under a variety of local stress states. This would be in-line with valley AE events observed due to compressive forces since a compressive force would most likely initiate the longitudinal and diagonal shear type cracking rather than tensile.
- The increased density of transverse cracks propagating especially through the 0 tow regions and MI matrix regions near the fracture surface appear to have strong interaction with the 90 tow cracking. Since the 90 tow regions are weaker, it would imply that they occur first and are the initiators of the transverse cracking – the same progression as would be inferred from valley AE occurring first and stimulating peak AE in Figure 9.

3.5 Comparison to 1 Hz and 0.01 Hz Fatigue

The two 1 Hz fatigue tests were similar to the 0.1 Hz fatigue test described above. The 1 Hz AE events had the same first peak directional character for peak (positive) and valley (negative) events. There are far more valley AE events and cumulative energy at the end of the test compared to peak AE activity. All events prior to the end of the test when valley events were observed were peak events. The frequency content and energy range behavior for valley events at the end of the test followed the same trend as for 113-3.

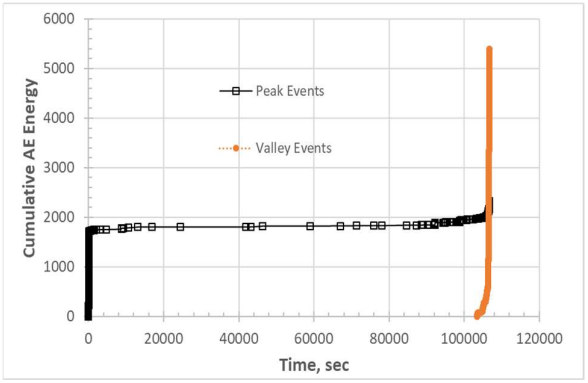

(a)

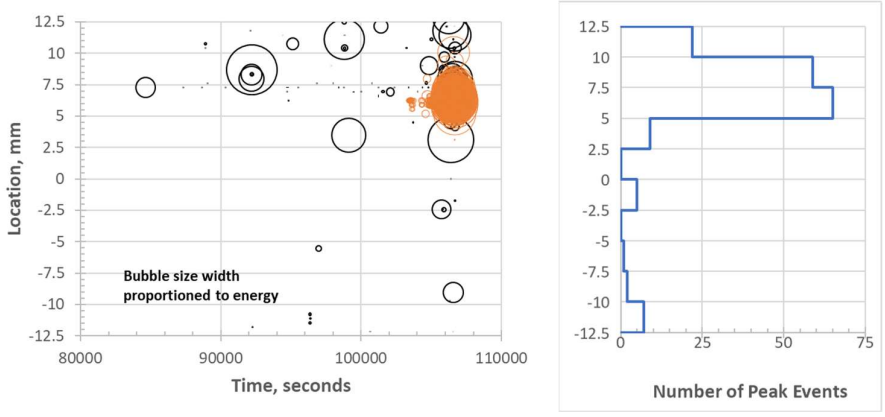

(b) (c)

Figure 11: AE activity for1 Hz fatigue specimen 147-3: (a) cumulative AE energy contributions from peak and valley events, (b) location of peak and valley events during the last part of the test and (c) histogram of peak event locations along the gage length.

Figure 11 shows the cumulative AE energy and location of peak and valley events for 147-3. There is one noticeable difference between the 1 Hz data and the 0.1 Hz data. For the 1 Hz data, there is significant peak events occurring prior to the onset of the valley events starting at ~ 84600 seconds (Figure 11a). Most of these events are low in energy and high in frequency. The valley events are centered at + 6.25 mm location (Figure 11b) whereas the peak events were centered at ~ +7.5 mm (Figure 11c). This corresponds with the region of fracture where there were two main "planes" for the fracture surface approximately 1 mm apart (Figure 12a). Some regions of longitudinal and diagonal cracking in the 90 tows as in the 0.1 Hz specimen were observed near the fracture surface on the lower half of the fracture surface shown in Figure 12a, which is a polished section close to the original edge of the tensile bar. The specimen was cut so that the surface longitudinal plane approximately 3.5 mm from the edge (Figure 12b) could be observed as well. Longitudinal cracking was pervasive near the fracture surface across the width in this region. Also prevalent in both regions was transverse matrix cracking through the 0 tow regions and MI matrix which appear to emanate from 90 tow cracks.

Since this specimen just prior to failure first had peak events occur in the failure region, most with high frequency and low energy, it is likely that these events corresponded to fiber breaks, as in other studies [16,25]. This would infer that local fiber breakage resulted in altering the stress-state in the specimen (for example if fiber breakage occurred on one half of the specimen) in the soon-to-be failure location which triggered the onset of "compressive" mechanisms which would then exacerbate peak stress damage leading to ultimate failure.

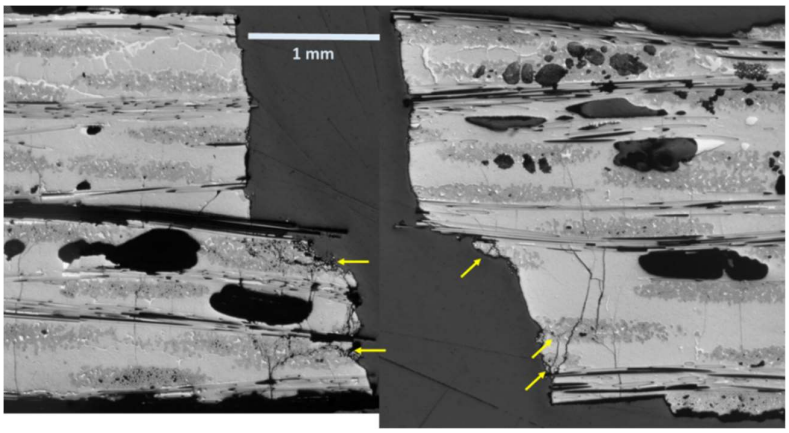

(a)

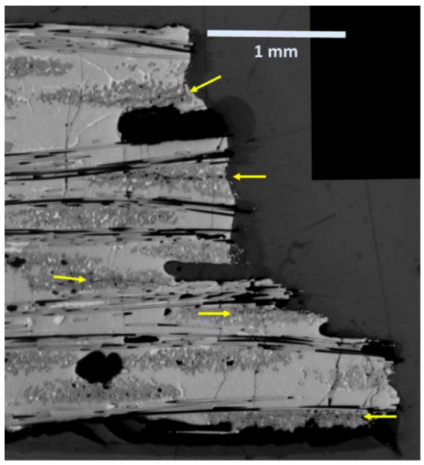

(b)

Figure 12: Polished longitudinal sections of 147-3: (a) both sides of the fracture surface approximately 1 mm from the edge and (b) the left side of the fracture surface approximately 3.5

mm from the edge of the specimen. Arrows indicate some of the longitudinal and diagonal cracking in the 90 tows.

For 0.01 Hz fatigue, valley events were not observed prior to failure. Figure 13a shows the AE activity of the last stress step leading to failure with significant AE activity in the failure region of +2.5 mm. Most of the events in this region are also low in energy (smaller bubble size in Figure 13a) and high in frequency (Figure 13b). This would infer a more common failure process where fiber breakage would cumulate locally leading to ultimate failure. Note that the fracture surface (Figure 14) does not show significant 90 tow damage other than one 90 longitudinal crack compared to the other two specimens (Figures 10 and 12).

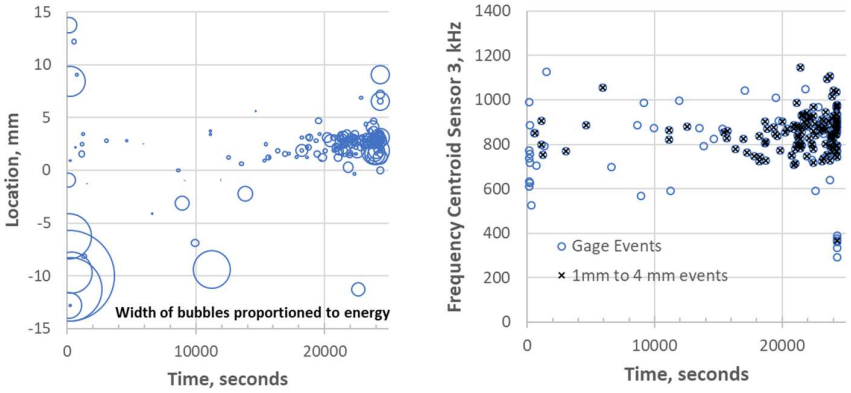

(a) (b)

Figure 13: Acoustic emission for 0.01 Hz tested 111-9 specimen: (a) location of AE at end of test and (b) frequency centroid of gage events at end of test.

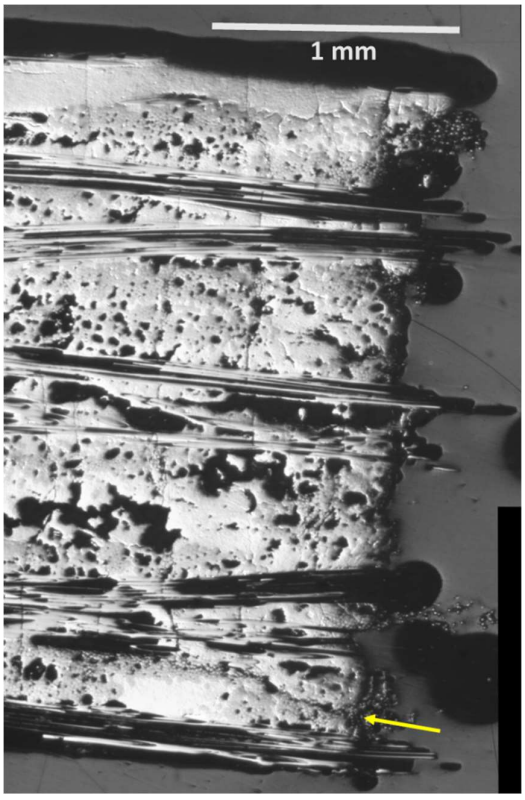

Figure 14: Fracture surface of 111-9.

4. Discussion

This study demonstrated different damage development, illuminated by the aid of acoustic emission, leading to failure for different fatigue frequency conditions on similar composites. The quality of the composites themselves were not very good including significant porosity; however, the methodology and findings are significant enough to merit further study and application to more advanced composite systems.

Essentially three different damage developments were observed. For the two composites examined subject to higher frequencies (0.1 and 1 Hz), a significant contribution to damage development leading to failure occurred in the unloading part of the fatigue cycle approaching and at the valley which exacerbated damage development on subsequent loading and peak portions of the fatigue test. The valley events only occurred in the region that was to fail within a few hours of ultimate failure. These valley events produced more AE energy at the very end of the test than all the AE events prior – a factor that appears to be a good indication that a valley mechanism is at work. However, what triggered the onset of valley events appears different for the two different experiments. The 0.1 Hz specimen appeared to have valley events form with little prior AE activity in the soon-to-be failure region so it was not clear what initiated the onset of valley events. The 1 Hz specimen had considerable peak AE events presumed to be fiber breakage leading up to the onset of valley events. The third type of fatigue failure did not have any valley events just prior to ultimate failure (0.01 Hz specimen) with significant low energy high frequency AE occurring near the peak of the stress cycle presumed to be cumulative fiber breakage leading to ultimate failure.

An attribute of the valley event waveforms that were captured by sensors a significant distance from the source was that the direction of the first peak was negative. This would mean that the front end of the extensional wave was dilated (tensile). This could only be caused by an event that was in compression. Microscopy showed that at and near the fracture surface, longitudinal and diagonal cracks were formed within the 90 tow regions (made up of the SiC fibers, BN interphase and CVI SiC sheath) of the woven architecture. These would correspond to local interlaminar and shear microfracture events within the 90 tow regions, respectively. The result of these local damage in the 90 tow regions would then result in transverse cracking in the 0 tow region and MI matrix due to the presence of new local transverse crack initiation sites resulting from the 90 tow damage as well as the redistribution of stress within the composite as the 90 tow region would effectively lose load-carrying ability.

A related issue to the valley mechanisms is there compressive nature while the composite was actually still subject to a global tensile stress (R = 0.1). For SiC/SiC MI composites, it is typical for the matrix to be in compression due the increase in volume that occurs when the liquid phase Si changes to solid Si [7]. After transverse matrix cracking at some tensile stress resulting in non-linear stress behavior and a hysteresis unload/reload stress strain behavior, materials with residual compression in the matrix exhibit stiffening in the unloading curve at low stresses [27]. The cause of the stiffening is due to crack closure upon unloading because when the matrix relieves the compressive stress at a matrix crack, the matrix is free to expand resulting in the two halves of the matrix contacting one another as stress approaches zero. Therefore, for these types of composites it is not surprising that a compressive force could be exerted in the region of the matrix crack on the matrix upon unloading. Also this would be enhanced by fatigue where sliding interfaces within the debonded region where fiber/matrix sliding occurs would lessen the frictional sliding stress resulting in further volume of matrix that could relieve its compressive residual stress [28]. In addition, the redistribution of local stress due to local fiber breakage and debris from interfacial wear could produce local high stress contact points during unloading leading to local 90 tow microfractures in compression. Of course the degree of compressive force upon unloading would depend on the R ratio and perhaps composite system. One would expect higher R ratios to not have the compressive types of mechanisms and negative R ratios to have worsening of the compressive mechanisms. Porosity may also play a role in the relief of matrix stress and/or creation of debris.

5. Conclusions

Acoustic emission was shown to be an excellent technique to identify the progression of damage accumulation in fatigue tests performed on woven SiC fiber reinforced SiC based matrix composites under three different frequency conditions. Failure in some cases was influenced by damage that occurred during the unloading portion of the fatigue cycle as well as fiber breakage during the loading to peak portion of the fatigue cycle. AE was able to discern the different progression and types of damage via location, energy, frequency and direction of the first extensional peak of the waveform.

Funding: This research was partially funded by a STTR program with Alphastar Corporation funded by NAVAIR, contract number N68335-12-C-0060, managed by Dr. Sung Choi.

Acknowledgments: The authors would like to thank Michael Presby for interesting discussions on the direction of the first peak of the extensional waves of AE waveforms.

Conflicts of Interest: The authors declare no conflict of interest.

References

1. Marshall, D.B. and Evans, A.G., Failure mechanisms in ceramic-fiber/ceramic-matrix-composites. *J. Am. Ceram. Soc.*, 1985, 68, 225-31.
2. Brooks, R. Tests show CMC parts 'breakthrough' for jet engines. *AmericanMachinist*, 2015, 9, (Sept.) http://americanmachinist.com/news/tests-show-cmc-parts-breakthrough-jet-engines.Engine component
3. Marshall, D.B., Cox, B.N., and Evans, A.G. The Mechanics of Matrix Cracking in Brittle Matrix Composites, *Acta Metall.*, 1985, 33. 2013-2021
4. Kim, R.Y. and Pagano, N.J., Crack initiation in unidirectional brittle matrix composites. *J. Am. Ceram. Soc.*, 1991, 74, 1082-1090.
5. Jenkins, M.G., Piccola, J.P., and Lara-Curzio, E. Onset of cumulative damage and the effects of test parameters on the tensile behavior of continuous fiber-reinforced ceramic composites (CFCC), in *Fracture Mechanics of Ceramics*, Vol. 12, edited by Bradt, R.C., Hasselman, D.P.H., Munz, D., Sakai, M. and Shevchenko, V. Y., Plenum Publishing, 1996, pp. 267–282.
6. Morscher, G.N., Modal Acoustic Emission of Damage Accumulation in a Woven SiC/SiC Composite, *Comp. Sci. Tech.* 1999, 59, 687-697.
7. Morscher, G.N. and Pujar, V.V. Design Guidelines for In-Plane Mechanical Properties of SiC Fiber-Reinforced Melt-Infiltrated SiC Composites, *Int. J. Appl. Ceram. Technol.* 2009, 6, 151-163.
8. Cox, B.N. and Marshall, D.B., Crack initiation in fiber-reinforced brittle laminates, J. Am. Ceram. Soc., 1996, 79, 1181-1188.
9. Morscher, G.N. Stress-Environmental Effects on Fiber-Reinforced SiC-Based Composites, Chapter 11 in Ceramic Matrix Composites: Materials, Modeling and Technology, Eds: Bansal, N.P. and Lamon, J. John Wiley and Sons: 2015. 334-352
10. Evans, A.G. and Zok, F.W., The physics and mechanics of fibre-reinforced brittle matrix composites, *J. Materials Science*, 1994, 29, 3857-3896.
11. Morscher, G.N., Stress-Dependent Matrix Cracking in 2D Woven SiC-fiber Reinforced Melt-Infiltrated SiC Matrix Composites, *Comp. Sci. Tech.*, 2004, 64, 1311-1319
12. Morscher, G.N., Singh, M., Kiser, J.D., Freedman, M., and Bhatt, R. Modeling Stress-Dependent Matrix Cracking and Stress-Strain Behavior in 2D Woven SiC Fiber Reinforced CVI SiC Composites, *Comp. Sci. Tech.*, 2007, 67, 1009-1017
13. Morscher, G.N., Yun, H.M., and DiCarlo, J.A. Matrix Cracking in 3D Orthogonal Melt-Infiltrated SiC/SiC Composites with Various Z-Fiber Types, *J. Am. Ceram. Soc.*, 2005, 88, 146-153
14. Morscher, G.N., Gyekenyesi, J.Z., and Gyekenyesi, A.L. Mechanical Behavior of Notched SiC/SiC Composites, ASME International Gas Turbine and Aeroengine Congress, June 4-7, 2001, No. 2001-GT-461
15. Morscher, G.N., Hurwitz, F. I. and Calomino, A. M. C-Coupon Studies of SiC/SiC Composites Part I: Acoustic Emission Monitoring, *Ceram. Eng. Sci. Proc.*, 2002, 23, 379-386

16. Morscher, G.N. and Gordon, N.A., Acoustic emission and electrical resistance in SiC-based laminate ceramic composites tested under tensile loading. J. Euro. Ceram. Soc., 2017, 37, 3861-3872 https://doi.org/10.1016/j.jeurceramsoc.2017.05.003
17. Baker, C., Morscher, G.N., Pujar, V.V. and Lemanski, J. R. Transverse cracking in carbon fiber reinforced polymer composites: modal acoustic emission and peak frequency analysis, *Comp. Sci. Tech.*, 2015, 116, 26-32; http//dx.doi.org/10.1016/j.compscitech.2015.05.005
18. Maillet, E., Baker, C., Morscher, G.N., Pujar, V.V., and Lemanski, J.R. "Feasibility and limitations of damage identification in composite materials using acoustic emission," *Composites A*, 2015, 75, 77-83, http//dx.doi.org/10.1016/j.compositesa.2015.05.003
19. Gorman, M.R. and Prosser, W.H., AE source orientation by plate wave analysis, *J. Acoustic Emission*, 1991, 9, 283-288.
20. Prosser, W.H., Jackson, K.E., Kellas, S., Smith, B.T., McKeon, J., Friedman, A. Advanced Waveform Based Acoustic Emission Detection of Matrix Cracking in Composites, *Materials Eval.*, 1995, 9, 1052–1058
21. Han, Z., Morscher, G.N., Maillet, E., Kannan, M., Choi, S.R., and Abdi, F. Electrical Resistance and Acoustic Emission During Fatigue Testing of Pristine and High Velocity Impact SiC/SiC Composites at Room and High Temperatures. Proceedings of ASME Turbo Expo 2016, GT2016-56507, June 13-17, 2016
22. Han, Z and Morscher, G.N., Monitoring fatigue of SiC/SiC ceramic matrix composites with acoustic emission. Proceedings of the ASME Turbo Expo 2019, GT2019-91330 submitted
23. Akaike, H., Markovian representation of stochastic processes and its applications to the analysis of autoregressive moving average process. *Ann. Inst. Stat. Math.* 1974, 26, 363-387.
24. Maillet, E. and Morscher, G.N. Waveform-based selection of acoustic emission events generated by damage in composite materials, *Mechanical Systems and Signal Processing*, 2015, 52-53, 217-227 http://dx.doi.org/10.1016/j.ymssp.2014.08.001
25. Morscher, G.N. and Maxwell, R., Monitoring tensile fatigue crack growth and fiber failure around a notch in laminate SiC/SiC composites utilizing acoustic emission, electrical resistance, and digital image correlation, J. Euro. Ceram. Soc., in press. https://doi.org/10.1016/j.jeurceramsoc.2018.08.049
26. Grosse, C.U. and Linzer, L.M., Signal-based AE analysis, in Acoustic Emission Testing, Eds, Grosse, C.U. and Ohtsu, M. Springer-Verlag: Berlin, 2008, pp. 77-79.
27. Domergue, J.M., Vagaggini, E., and Evans, A.G., Relationships between hysteresis measurements and the constituent properties of ceramic matrix composites: II, experimental studies on unidirectional materials, *J. Am. Ceram. Soc.*, 1995, 78, 2721-31.
28. Rouby, D. and Reynaud, P. Fatigue behavior related to interface modification during load cycling in ceramic matrix fibre composites, *Comp. Sci. Tech.*, 1993, 48, 109-118.